122.6 Tb/s S+C+L Band Unrepeatered Transmission over 223 km Link with Optimised Bidirectional Raman Amplification

Jiaqian Yang, Henrique Buglia, Mindaugas Jarmolovičius, Romulo Aparecido, Eric Sillekens, Ronit Sohanpal, Mingming Tan, Dini Pratiwi, Ruben S. Luis, Benjamin J. Puttnam, Yuta Wakayama, Ralf Stolte, Wladek Forysiak, Polina Bayvel, and Robert I. Killey

(Top-scored Paper)

***Abstract*—A 223 km unrepeatered link transmission is experimentally demonstrated, transmitting 490 polarisation-division multiplexed channels with adaptively optimised geometrically-shaped constellation quadrature amplitude modulation signals. The transmission band covered nearly the entire S-, C-, and L-bands, spanning 121 nm (15.6 THz) of optical bandwidth. Lumped Thulium- and Erbium-doped fibre amplifiers were used for amplification, and bidirectional distributed Raman amplification, together with pre-emphasis of signal launch power spectrum, were used to mitigate the interchannel stimulated Raman scattering (ISRS) effect. The signal power pre-emphasis and the powers of the Raman pumps were experimentally optimised with a differential evolution algorithm to improve the received signal-to-noise ratio and the throughput. The closed-form ISRS Gaussian noise model was used to support and explain the experimental results: it accurately reproduces the evolution of the signal spectral power and estimates the contributions of nonlinear interference noise and amplified spontaneous emission noise in the unrepeatered link. The combined use of the hybrid amplification scheme, adaptive constellation shaping, and system optimisation techniques resulted in a total throughput of 122.62 Tb/s, from the generalised mutual information (113.95 Tb/s after decoding), achieving the highest throughput to date for unrepeatered links over 200 km.**

***Index Terms*—unrepeatered transmission, ultra-wide band transmission, inter-channel stimulated Raman scattering, distributed Raman amplification.**

I. Introduction

UNREPEATERED systems have been proposed as a solution for establishing transmission links spanning several hundred kilometres without the need for in-line amplifiers. This is particularly useful for global submarine systems, where electrically powered components, such as optical repeaters, are difficult to deploy [1]. The cost and power consumption restrict the deployment of new links between remote locations, and the growth in data demand, driven by cloud computing and data streaming, necessitates further throughput increase within the existing fibre infrastructure. This can be achieved by bandwidth expansion beyond the widely-deployed C-band. The use of the S-band and L-band has been proposed to extend the transmission bandwidth and throughput over a single span of fibre [2]. In unrepeatered systems, however, due to the long transmission distance, significant fibre attenuation and the interchannel stimulated Raman scattering (ISRS) effect become dominant impairments compared to dispersive and Kerr nonlinear effects, making it challenging to expand the wavelength-division multiplexing (WDM) optical bandwidth in such systems. Achieving wider bandwidths requires careful selection of appropriate amplification schemes for signals in each band and effective management of the ISRS power transfer.

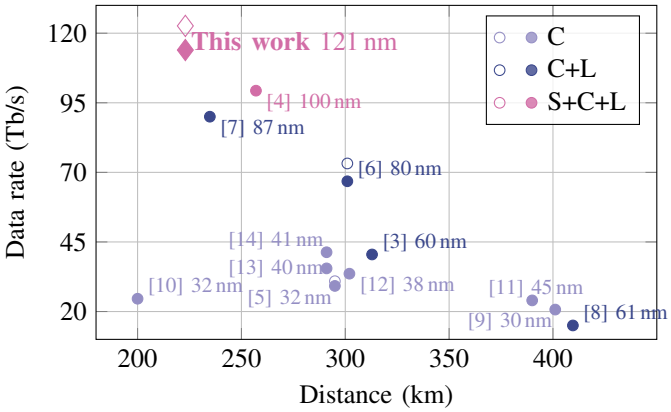

Fig. 1: Transmission distance, total throughput, and used bandwidth of recent unrepeatered transmission demonstrations. Solid markers: decoded net rate; Open markers: rate from generalised mutual information (GMI).

Novel amplification technologies [3], [4], advanced modulation formats [5], [6], and system optimisation techniques [7] have significantly extended the capacity and reach of unre-

Manuscript received XX XX, XXXX; revised XX XX, XXXX.

This work was supported by EPSRC grants EP/R035342/1 Transforming Networks - building an intelligent optical infrastructure (TRANSNET), EP/W015714/1 Extremely Wideband Optical Fibre Communication Systems (EWOC), EP/V000969/1 All-Raman optical amplification for next Generation ultra-wideband Optical Networks (ARGON), EP/V007734/1 EPSRC Strategic equipment grant, and EPSRC studentship (EP/T517793/1). The Microsoft 'Optics for the Cloud' Alliance support is acknowledged. The authors would like to thank Dr Sergejs Makovejs (Corning Inc.) for loan of the SMF-28 ULL fibre.

J. Yang, H. Buglia, M. Jarmolovičius, R. Aparecido, E. Sillekens, R. Sohanpal, P. Bayvel, and R. I. Killey are with Optical Networks Group, Department of Electronic and Electrical Engineering, UCL (University College London), London, UK (E-mail: jiaqian.yang.18@ucl.ac.uk)

M. Tan, D. Pratiwi, and W. Forysiak are with Aston Institute of Photonic Technologies, Aston University, Birmingham, B4 7ET, UK.

R. S. Luis and B. J. Puttnam are with National Institute of Information and Communications Technology, Koganei, Japan.

Y. Wakayama is with KDDI Research, Fujimino, Japan.

R. Stolte is with Coherent / Finisar, New South Wales, Australia.

peatered systems. Experiments with C-band and C+L-band configurations have achieved unrepeatered transmission distances exceeding 400 km and data rates of up to 66.8 Tb/s [5]–[14]. By including the L-band, a trade-off between throughput and transmission distance should be expected. For example, a higher throughput of 90.4 Tb/s was transmitted over a shorter link of 234.8 km using a bandwidth of 87.2 nm [7], while a longer transmission distance of 312 km was achieved using 60 nm C+L-band erbium-doped tellurite-fibre amplifiers, but with a lower throughput of 40.5 Tb/s [3]. Using standard C- and L-band erbium-doped fibre amplifiers (EDFAs), bi-directional distributed Raman amplification (DRA), and ultra-low loss G.654.E fibre, a real-time probabilistically-shaped constellation 64 quadrature amplitude modulation (QAM) unrepeatered transmission was demonstrated, achieving a net data rate of 66.8 Tb/s [6]. Further extension of the transmission bandwidth in unrepeatered links to include the S-band involves the use of wideband amplifiers, such as semiconductor optical amplifiers (SOAs) [15], and DRA, a distributed amplification technique widely used in ultra-wide band (UWB) single-span and long-haul transmission [2], [16]. A 2022 experiment employing a 100 nm bandwidth SOA and bi-directional DRA reported an unrepeatered transmission covering the longer-wavelength S-band, in addition to the C- and L-bands, achieving a throughput of 99.35 Tb/s over a distance of 257 km [4]. These recent demonstrations of unrepeatered transmission are summarised in Fig. 1. To fully utilise the S+C+L band in unrepeatered transmission, optimisation of the system parameters, including launch signal power and Raman pump wavelengths and powers, is essential. The estimation of throughput in UWB systems commonly uses the nonlinear Gaussian noise (GN) model [17], [18]. In recent years, several closed-form ISRS GN models that support arbitrary Raman amplification have been proposed [19]–[21]. These models aim to predict throughput and optimise systems in UWB transmission covering the S+C+L band and beyond.

This paper builds upon our work reported in [22], demonstrating a record 122.6 Tb/s S+C+L band transmission over a 223 km unrepeatered link, and specifically focuses on techniques for optimising launch signal power pre-emphasis and Raman pump powers in unrepeatered links. The experimental results are further supported by the closed-form ISRS GN model [20], [21], which quantifies and differentiates the impacts of amplified spontaneous emission (ASE) noise and nonlinear interference (NLI) noise. The model explains the severe ASE limitation and the need to mitigate it using Raman amplification in unrepeatered systems. Comprehensive analysis of signal power evolution and the different noise contributions to the received signal-to-noise ratio (SNR), including ASE noise from both Raman and lumped amplification, and NLI noise, in the presence of co- and counter-propagating Raman pumps, is included. The study highlights the necessity of system optimisation to balance the ASE noise, ISRS and NLI noise arising in unrepeatered systems. The paper is organised as follows: Section II describes the unrepeatered transmission experimental setup, including the Raman pumps and fibres used in this study. Section III details the Raman pump power optimisation technique using the differential evolution (DE) algorithm. Section IV presents the main experimental results along with SNR predictions and analyses from the closed-form ISRS GN model. Finally, conclusions are given in Section V.

II. Experimental Setup

The experimental setup of the S+C+L UWB unrepeatered transmission is shown in Fig. 2. Three optical carriers with < 100 kHz linewidth were generated by external cavity lasers (ECLs) with frequency spacing of 32.5 GHz. The carriers were amplified by either S-band thulium-doped fibre amplifiers (TDFAs) or C / L-band polarisation-maintaining EDFAs, depending on the operating optical band. Polarisation alignment was carried out only for S-band carriers, since the TDFA was not polarisation-maintaining. The centre channel and the neighbouring channels were modulated with 32 GBaud digitally pre-distorted root-raised-cosine (RRC) shaped signals with 1 % roll-off by dual polarisation (DP) - in-phase quadrature (IQ) modulators (35 GHz bandwidth), each driven by amplified waveforms from a 92 GSa/s arbitrary waveform generator (AWG) with 8-bit vertical resolution (5 bit ENOB). The signal comprised repeating blocks of 65,536 randomly generated symbols, with quadrature phase shift keying (QPSK) pilots inserted. The digital pre-distortion mitigated the frequency roll-off of the AWG and the modulator with a linear filter [23]. Two 2 % taps were inserted after the modulator to monitor the optical power which provided feedback to the polarisation controller. After the booster amplifiers, the three signal channels were swept across the transmission optical bands in a frequency grid of 32.5 GHz, with the centre channel being used to assess the transmission performance, and the neighbouring channels being interfering dummy channels. A variety of geometrically-shaped (GS) constellations were used in each optical band according to the channel SNR [24].

The other co-propagating WDM channels were emulated using UWB spectrally-shaped amplified spontaneous emission (SS-ASE) noise. The ASE noise was generated by an UWB ASE source, spectrally-shaped using Coherent WaveShapers® operated as wavelength selective switches (WSSs) in a double-pass configuration and two-stage amplified to produce a flat or pre-emphasised spectrum. A notch was carved by the WSS, within which the three signal channels were positioned. The use of wide-band ASE noise to emulate aggressor channels provides a conservative measure of the transmission performance, and this technique has been previously validated [25], [26] and widely used [2], [4], [16], [27], [28]. The insets in Fig. 2 show an example of the shaped and pre-emphasised launch signal power spectrum profile (with a 15 dB tilt across the three bands) and the three signal channels placed within the sliding notch. The SS-ASE and signal channels were combined using a 90:10 power coupler, with 90 % power from the SS-ASE and 10 % from the signals. In the following experiment, the power of the signal channels was further attenuated to match the SS-ASE power density. Based on the SS-ASE bandwidth and the wavelength tunability of the lasers, the channel-under-test could cover the wavelength ranges of 1470 nm to 1526 nm in the S-band, 1531 nm to 1565 nm in the C-band, and 1572 nm to 1608 nm in the L-band, resulting in 228×, 132×, and 130× WDM channels per band respectively.

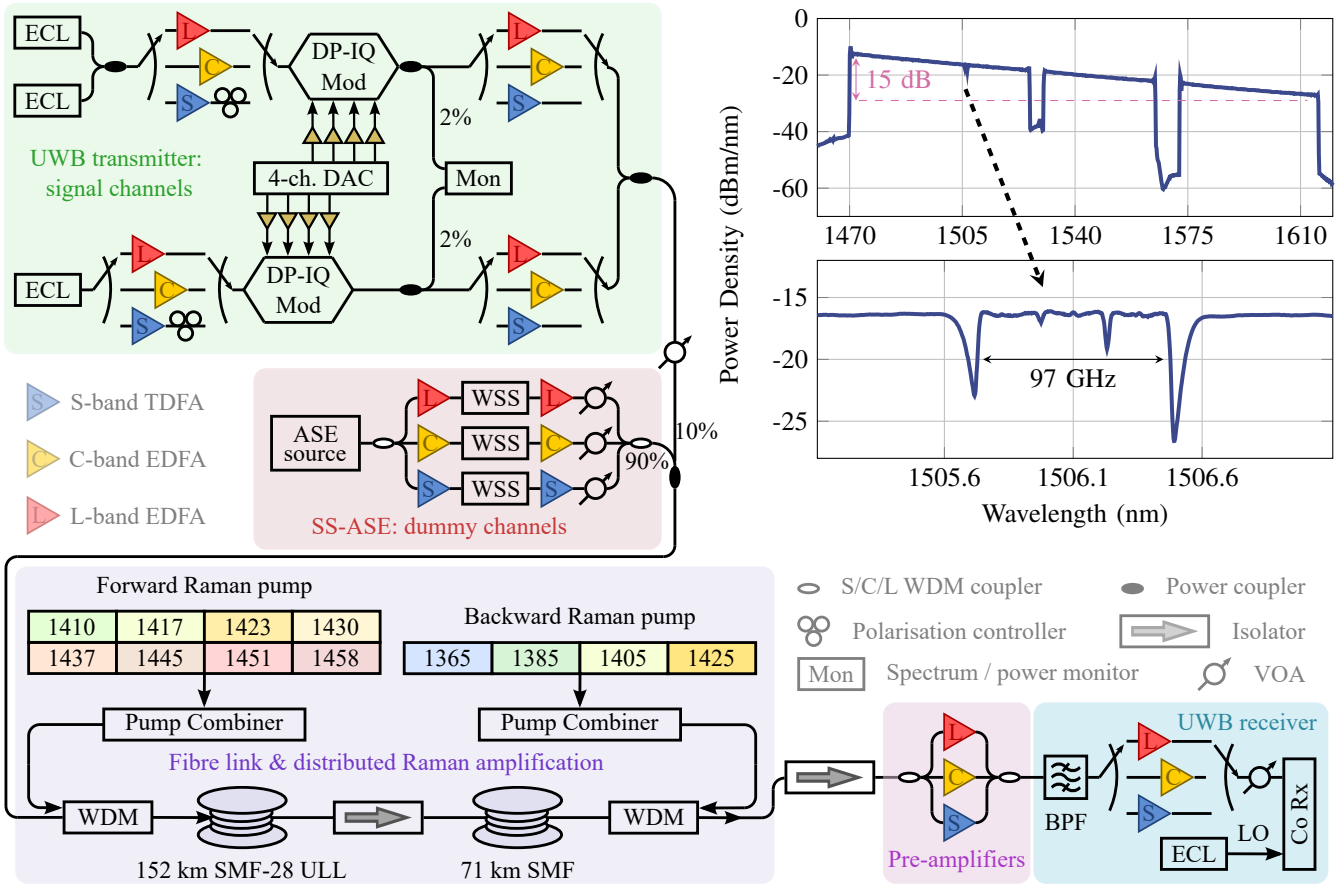

Fig. 2: Experimental setup for S+C+L band unrepeatered transmission over 223 km with bidirectional distributed Raman amplification. Insets: Top: shaped launch power spectrum with pre-emphasis of 15 dB tilt; Bottom: 3×32 GHz signal channels being placed within the notch.

The transmission link consisted of 152 km of ultra-low-loss (ULL) 83 micrometre square effective area fibre followed by 71 km of G.652.D low water peak single-mode fibre (SMF). The ULL fibre is ITU-T G.652.B-compliant SMF with minimum attenuation of 0.16 dB/km at 1550 nm. The low water peak SMF has reduced attenuation in the E-band. Total loss of the transmission link was 37.2 dB at 1550 nm. The forward and backward Raman pump wavelengths λ are listed in Table I. The forward Raman pumps cover the wavelength range of 1410 nm to 1458 nm, mainly enhancing the optical signal-to-noise ratio (OSNR). The maximum available pump powers are around 250 mW for the first two wavelengths and 130 mW for the remaining wavelengths. The backward Raman pumps emit at shorter wavelengths and provide significant Raman gain in the S-band to offset the ISRS-induced power transfer from the S-band to the L-band. The efficiency of backward DRA was ensured by using high-power pumps (maximum power of more than 500 mW each) and propagating in a low water peak fibre, to maintain fibre attenuation below 0.3 dB/km at pump wavelengths, as illustrated in Fig. 3(a). The Raman gain profile, measured at pump wavelength of 1456 nm, is depicted in Fig. 3(b). These fibre parameters were used in the modelling in Section IV. Lumped pre-amplifiers (with noise figures of 7 dB, 5 dB, and 5.5 dB for S-TDFA,

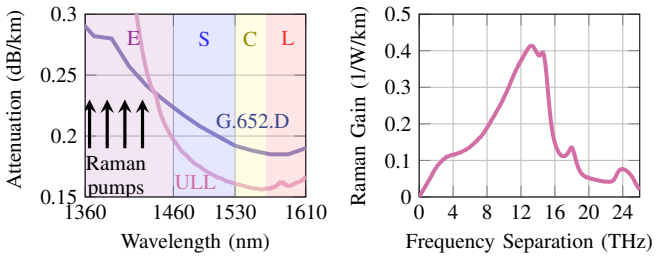

Fig. 3: (a) Attenuation of the two types of single-mode fibres. (b) Raman gain profile.

C-EDFA, and L-EDFA, respectively) were positioned at the end of the fibre link, followed by the UWB receiver.

At the receiver, the channel under test was selected using a tunable optical band pass filter (BPF). The channel power was boosted by another amplifier in the corresponding band, and a variable optical attenuator (VOA) was used to control the power into the receiver. A coherent receiver detected the DP-IQ signal using an optical hybrid with a local oscillator (LO). A 256 GSa/s 110 GHz Keysight UXR digital oscilloscope with a 10-bit ADC (approximately 5-bit ENOB at 70 GHz) was used to digitise and capture the waveform, following

which pilot-based DSP was carried out [29]. Transmission performance was quantified from the SNR and generalised mutual information (GMI) calculated based on the log-likelihood ratios [30] after deducting the pilot overhead of 4.64 %. DVB-S2X low-density parity check (LDPC) codes were used to decode the received symbols [31] with adaptive code rate, and code-rate puncturing was applied to achieve a bit error rate below 3×10^{-4} with a 0.5 % overhead BCH code.

III. System Optimisation

Before transmission, the optimisation of the Raman pump powers and the launch signal power pre-emphasis was carried out. First, the received SNR was estimated by carving 25 notches in the SS-ASE without signal loading (as shown in Fig. 4(a)), transmitting the SS-ASE through the fibre link, and measuring the received notch depth (as depicted in Fig. 4(b) and inset), which approximately represented the SNR. The SNR was then interpolated to estimate values for all channels and mapped to capacity using the Shannon capacity theorem. It is important to highlight that the estimated SNR derived from notches considers the impact of ASE noise accumulation and ISRS but does not account for nonlinear interference noise or transceiver noise. This approach is particularly effective for unrepeatered systems, as their performance is primarily limited by ASE noise. Using this throughput estimation as a metric, the differential evolution (DE) algorithm [32], [33] was used to optimise the launch power tilt and bidirectional pump powers.

In the initialisation stage of the DE, a population of 10 random combinations of the 8 forward pumps and 4 backward pumps powers are generated:

$$\begin{aligned}\vec{\mathbf{p}}_1 &= [p_{1,1}, p_{1,2}, \cdots, p_{1,12}] \\ &\cdots \\ \vec{\mathbf{p}}_{10} &= [p_{10,1}, p_{10,2}, \cdots, p_{10,12}]\end{aligned} \tag{1}$$

In each iteration, an agent combination $\vec{\mathbf{p}}_i = [p_{i,1}, p_{i,2}, \cdots, p_{i,12}]$ is randomly selected. A mutant vector $\vec{\mathbf{q}} = [q_1, q_2, \cdots, q_{12}]$ is generated from another three vectors through linear combination:

$$\vec{\mathbf{q}} = \vec{\mathbf{p}}_k + F(\vec{\mathbf{p}}_m - \vec{\mathbf{p}}_n), \quad k, m, n \neq i \tag{2}$$

Here, F is the mutation rate. Uniformly distributed random numbers $u_1, u_2, \cdots, u_{12}$ are generated for each dimension, and the trial vector $\vec{\mathbf{t}} = [t_1, t_2, \cdots, t_{12}]$ is produced from either the agent or the mutant following the rule:

$$\begin{cases} t_i = p_{i,j} & \text{if} \quad u_j \geq \text{cr} \\ t_i = q_i & \text{if} \quad u_j < \text{cr} \end{cases} \tag{3}$$

Here, cr is the crossover rate that controls the probability of mixing the components of different candidate solutions to create a new one. Higher crossover rate means that more components from the mutated vector are incorporated into the trial vector. This trial vector is then used to assess the system performance. If the trial vector performs better, the agent is replaced by the trial. Otherwise, the agent remains unchanged. This process is repeated for each vector in the population to complete an iteration. After 10 iterations, the best-performing vector from the final population is considered as the optimised result. A population size of 10 individuals, a mutation rate of 0.5, and a crossover rate of 0.7 were used.

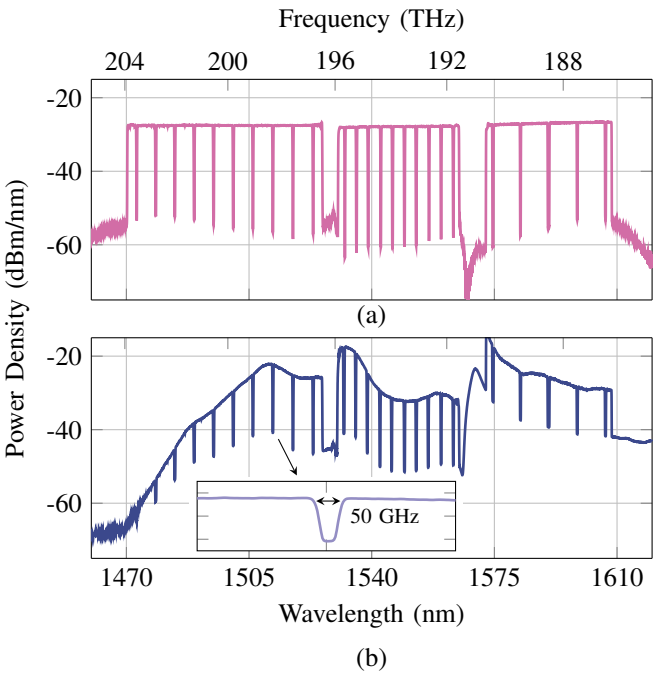

Fig. 4: SS-ASE spectra with multiple notches in the pump optimisation process. (a) Transmitted; (b) Received. Inset: received notch with a depth approximately representing the received SNR.

The optimisation was carried out for each launch power tilt (ranging from 0 dB to 25 dB in 5 dB steps). The best performance was observed with a 15 dB launch power tilt, and the optimised pump powers P_{opt} are listed in Table I. The total powers of the forward and backward Raman pumps were 1.14 W and 1.69 W, respectively.

Transmitted and received SS-ASE spectra with multiple notches were measured using an optical spectrum analyser (OSA) with a 0.02 nm resolution bandwidth in a high-

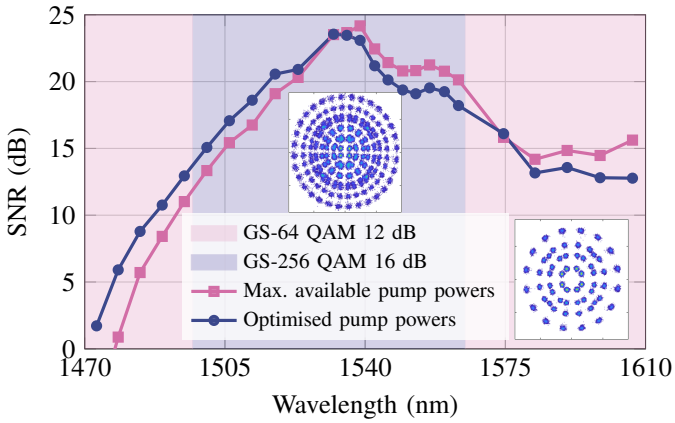

Fig. 5: Estimated received SNR in the optimisation process and the choice of different constellation shaping methods.

TABLE I: Raman pumps configuration.

	Forward Pumps								Backward Pumps				Total
λ (nm)	1410	1417	1423	1430	1437	1445	1451	1458	1365	1385	1405	1425	
P_{opt} (mW)	267.3	247.2	134.3	128.5	130.3	73.6	49.0	111.7	503.5	503.5	455.0	231.7	**2,836**

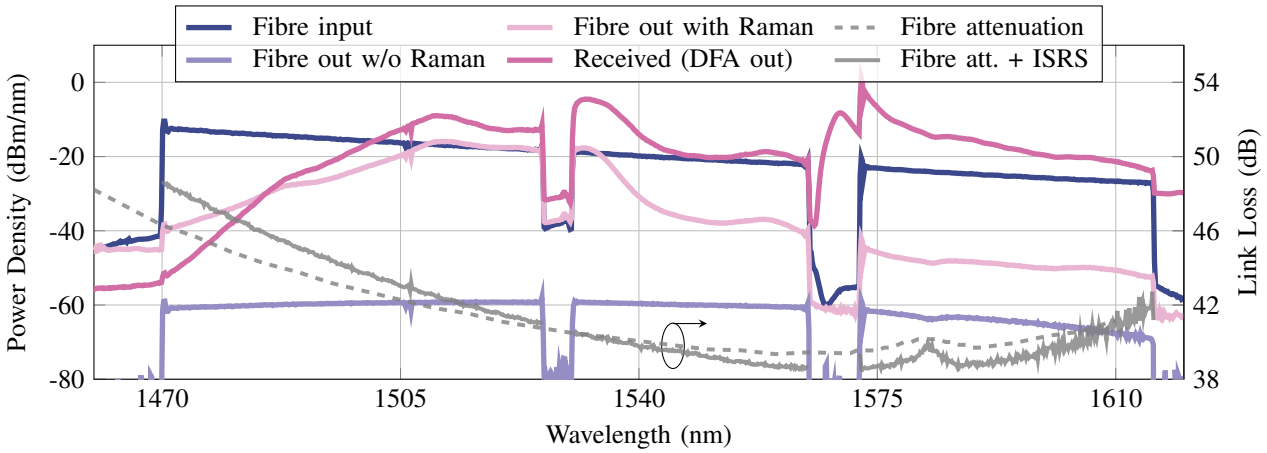

Fig. 6: Signal power spectra measured by OSA and link loss. DFA: doped fibre amplifers. Dashed gray line: wavelength-dependent fibre attenuation from fibre specifications; solid gray line: link loss accounting for fibre attenuation and ISRS, calculated from the measured spectra.

sensitivity mode, and the results are shown in Fig. 4. The notches in the spectrum show a transmitted SNR of 20-35 dB across the S+C+L band, which largely degrades to 5-20 dB in the S-band after unrepeatered transmission due to the ASE noise arising from the Raman amplification and pre-amplifier TDFA used to offset the fibre loss and the ISRS effect. The C-band SNR has a relatively low reduction after transmission, to the range of 20-25 dB. This is because the noise figure of the C-EDFA (approximately 5 dB) is the lowest among the three types of lumped amplifiers, and part of the C-band signal benefits from the Raman amplification, whereas the L-band SNR is around 13 dB, relatively lower than that in the C-band because of the ASE noise from the significant gain of nearly 40 dB provided by the lumped L-EDFAs. This SNR degradation arising from the ASE noise is also predicted by the model, as described in Section IV. Figure 5 shows the received SNR measured from the notches for different wavelengths per band, for both the maximum and optimised pump powers. The SNR increased by 2.63 dB, on average, in the S-band, enabling higher throughput to be achieved by reducing pump powers and reducing ISRS, at the cost of slightly worse performance in the C- and L-bands (1.24 dB reduced SNR), resulting in an increase in the estimated total capacity from 152.6 Tb/s to 155.3 Tb/s. The figure also shows the geometrically-shaped modulation formats transmitted for each channel, optimised for the channel SNR [24], e.g. GS-64 QAM optimised for a 12 dB SNR channel for shorter wavelength S-band and L-band, and GS-256 QAM optimised for a 16 dB SNR channel for longer wavelength S-band and C-band. The format selected depended on the estimated channel SNR at the each wavelength.

IV. Result and Discussion

The signal spectra at the input and output of the transmission link were measured using an OSA with a 0.02 nm resolution bandwidth, and the results are shown in Fig. 6, along with the fibre attenuation and link loss calculated based on the fibre specifications and the measured spectra. The launch powers were 19.6 dBm, 12.2 dBm, and 8.6 dBm for the S-, C-, and L-bands, respectively, with the signal channel power attenuated to match the SS-ASE power spectral density. After transmission over 223 km of single-mode fibre without Raman amplification, the signal power was attenuated by the joint effect of wavelength-dependent fibre loss and ISRS. The minimum link loss was measured to be 38.5 dB (including the insertion loss of the isolator) at 1573 nm, while in the S-band, losses could extend up to 48 dB, with an additional 2 dB power loss being attributed to ISRS. The bi-directional Raman amplified spectrum and received spectrum after lumped amplification are also plotted in Fig. 6. The received signal power is restored to values similar to the launch powers at most wavelengths, except for the lower half of the S-band due to the significant link loss and the power-dependent gain profile of the TDFAs.

The maximum Raman on/off gain of more than 30 dB was observed in the S-band with backward Raman pumps only, and more than 40 dB with bidirectional Raman pumps, as shown in Fig. 7. The strong backward Raman pumps with output powers of around 500 mW each and wavelengths of 1365 nm - 1425 nm provide significant Raman gain for the entire S-band, peaking at 1510 nm. The forward Raman pump wavelengths ranged up to 1458 nm, causing a power transfer peak around mid-C-band, and an additional gain of about 10 dB was simultaneously observed across the L-band. A slight reduction in gain at the lower wavelengths of the S-band was noted when forward pumps were added, due to stronger ISRS power transfer from the S- to the L-band. This trade-off between the S- and L-band power spectral densities justifies the necessity of optimising the launch power tilt and Raman

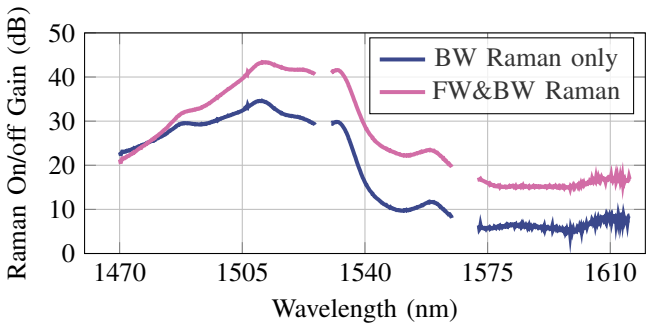

Fig. 7: Raman amplification on/off gain. FW: forward; BW: backward.

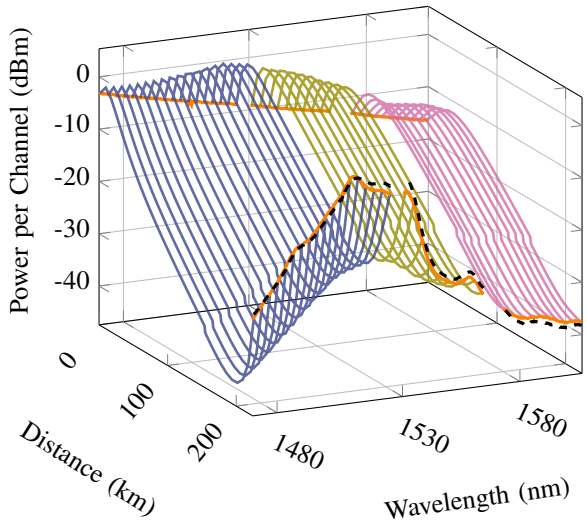

Fig. 8: Signal power evolution in the 223 km transmission estimated from the differential coupled Raman equations (solid lines) and measured received spectrum (black dashed line).

pump powers.

The closed-form ISRS GN model for UWB transmission with distributed amplification was used to model the unrepeatered link and give a prediction of the signal power evolution and the contributions of different noise to the total SNR. The goal is to differentiate between ASE and NLI noise in the link and demonstrate the benefits of using distributed amplification to reduce ASE noise from lumped amplifiers. The model treats the impairments which originate from fibre nonlinearity, amplifier noise and transceiver noise as additive noise terms, such that the total received SNR is given by

$$\mathrm{SNR}_{\mathrm{tot},i}^{-1} \approx \mathrm{SNR}_{\mathrm{TRx}}^{-1} + \mathrm{SNR}_{\mathrm{NLI}}^{-1} + \mathrm{SNR}_{\mathrm{ASE}}^{-1} \tag{4}$$

$$= \left(\frac{P_i}{\kappa_i P_i + \eta(f_i) P_i^3 + P_{\mathrm{ASE},i}} \right)^{-1}, \tag{5}$$

where $\mathrm{SNR}_{\mathrm{TRx}}$, $\mathrm{SNR}_{\mathrm{NLI}}$ and $\mathrm{SNR}_{\mathrm{ASE}}$ are the SNR from the transceiver subsystem, the nonlinear interference (NLI) noise, and the ASE noise from the optical amplification, respectively. i is the index of the channel under consideration, P_i is the channel launch power, $\kappa_i = 1/\mathrm{SNR}_{\mathrm{TRx},i}$, and $P_{\mathrm{NLI},i} = \eta(f_i)P_i^3$ is the NLI noise power, $\eta(f_i)$ is the nonlinear coefficient at optical frequency f_i. $P_{\mathrm{ASE},i} = G_i P_{\mathrm{ASE}'',i} + P_{\mathrm{ASE}',i}$ is the total ASE noise contributed from Raman amplification $P_{\mathrm{ASE}'',i}$ and lumped amplification $P_{\mathrm{ASE}',i}$ where G_i is the lumped EDFA or TDFA gain.

The wavelength-dependent fibre parameters, i.e. effective areas A_{eff}, Raman gains g_R, and nonlinear coefficients γ, were calculated in the model using the following equations from [34]:

$$\frac{A_{\mathrm{eff}}(f_i)}{A_{\mathrm{eff}}(f_{\mathrm{ref}})} = \left(\frac{f_i}{f_{\mathrm{ref}}} \right)^{-n_A} \tag{6}$$

$$\frac{g_R(f_i)}{g_R(f_{\mathrm{ref}})} = \left(\frac{f_i}{f_{\mathrm{ref}}} \right)^{1+0.1+n_A} \tag{7}$$

$$\gamma(f_i) = \frac{2\pi n_2 f_i}{A_{\mathrm{eff}}(f_i) c} \tag{8}$$

Here, f_{ref} is the reference frequency at 1550 nm, $n_A \approx 0.9$ for ultra-low-loss 83 micrometre square fibre and $n_A \approx 1.4$ for G.652.D single-mode fibre are the effective area scaling exponents [34], n_2 is the nonlinear refractive index. Reference effective areas of the ultra-low-loss 83 micrometre square fibre and the G.652.D single-mode fibre are 83 μm^2 and 80 μm^2, respectively. The insertion losses of the WDM couplers and isolators within the fibre link were estimated by employing nonlinear minimum search function in MATLAB® representing the error between the calculated and measured spectra across three different pumping schemes: without Raman amplification, with backward pumps only, and with bi-directional Raman pumps. The insertion losses of 0.2∼1.6 dB are estimated, which are within the manufacturers' specifications.

We assume cumulative fibre link dispersion of $D = 16.5$ ps $\cdot$ nm^{-1}km^{-1} at 1550 nm, and dispersion slope of $S = 0.09$ ps $\cdot$ nm^{-2}km^{-1}. The attenuation and Raman gain profile are shown in Fig. 3, and these data were used in the model to simulate the signal spectral power evolution along the 223 km fibre link, taking into account the forward and backward Raman pump and pump power depletion. As shown in the power evolution in Fig. 8, the contribution of forward Raman pumps is observed in the first 30 km transmission, while the backward pumps provide significant gain in the last 50 km of G.652.D fibre. The power drop at 152 km is caused by the insertion loss of the isolator (∼1.2 dB) placed at the mid-link. The mean error between the calculated channel powers at the end of the fibre and the experimentally measured values is 0.86 dB.

The NLI noise and ASE noise were evaluated using the closed-form ISRS GN model [20], [21], with the various noise contributions to the total SNR plotted in Fig. 9. ASE noise is the predominant contributor, which is divided into ASE from Raman amplification ($\mathrm{SNR}_{\mathrm{ASE,Raman}}$) and ASE from lumped amplification ($\mathrm{SNR}_{\mathrm{ASE,Lumped}}$), as shown in Fig. 9(a). The gain from lumped amplification was determined using experimentally measured spectra before and after lumped amplification, and $\mathrm{SNR}_{\mathrm{ASE,Lumped}}$ was estimated from the received signal power and lumped ASE noise power. From Fig. 6, the L-band requires the highest lumped gain, resulting in the lowest $\mathrm{SNR}_{\mathrm{ASE,Lumped}}$, which in turn limits the $\mathrm{SNR}_{\mathrm{ASE,tot}}$ in the L-band. The S-band, having the least lumped amplification

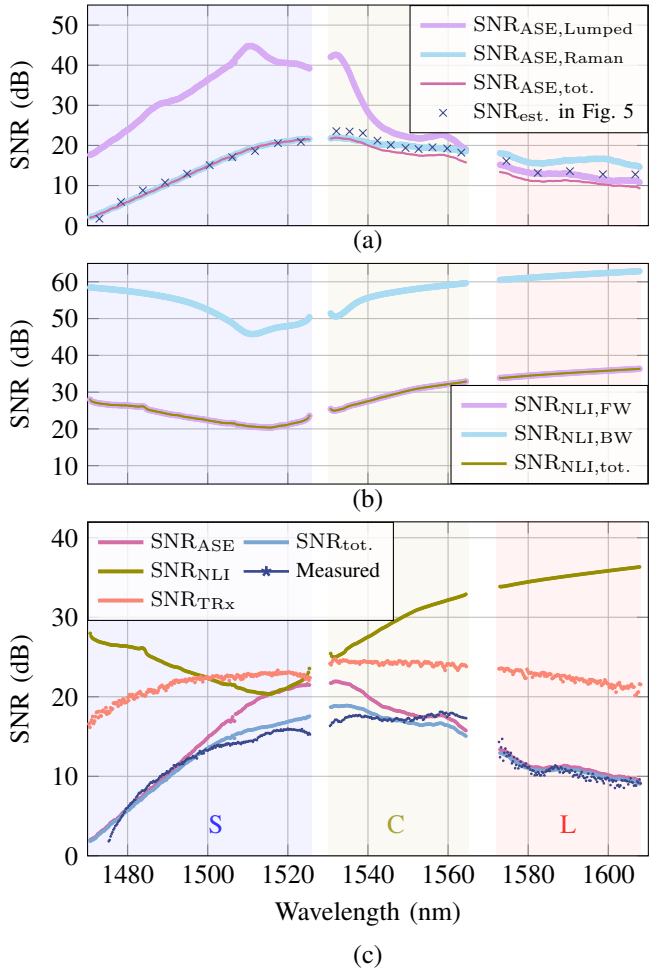

Fig. 9: Simulation and experimental results of received SNR. (a) Simulation results of total ASE noise contribution $\mathrm{SNR}_{\mathrm{ASE,tot}}$ from distributed Raman amplification and lumped amplification. (b) Simulation results of total NLI noise contribution $\mathrm{SNR}_{\mathrm{NLI,tot}}$ from forward (FW) and backward (BW) Raman amplification. (c) Simulation and experimental results of total SNR calculated from ASE-, NLI-, and transceiver-limited SNR. Star markers: experimentally measured SNR.

gain, thus experiences minimal ASE, but its $\mathrm{SNR}_{\mathrm{ASE,Lumped}}$ is constrained by the low received signal power. For ASE from Raman amplification, the S-band and C-band signals receive the highest Raman gain. Consequently, $\mathrm{SNR}_{\mathrm{ASE,tot}}$ is limited by $\mathrm{SNR}_{\mathrm{ASE,Raman}}$. Although the L-band has the least Raman gain and the least ASE from Raman amplification, this ASE noise was further amplified by the significant lumped gain, resulting in an $\mathrm{SNR}_{\mathrm{ASE,Raman}}$ comparable to that of the S- and C-bands. Compared with the experimentally estimated SNR values shown in Fig. 5, both methods provide the ASE-limited SNR. The slight discrepancies observed in the C- and L-bands can be attributed to the accuracy of power spectrum evolution predictions in the model and other differences between the modelled and experimental parameters, such as the wavelength-dependent amplifier noise figure, estimation of component insertion losses, and difficulties in precise power measurement.

The NLI noise contribution is calculated separately for the two sections of fibre links, with forward Raman pumps being used exclusively in the first 152 km link and backward Raman pumps only in the last 71 km link. This assumption holds because the forward pumps deplete rapidly and become negligible in the second half of the link, while the isolator prevents any backward pump leakage into the first 152 km of the link. Due to the reduced signal power, the interaction between NLI noise in the second half is minimal, allowing the NLI-limited SNR from forward pumping to be directly calculated using the reference signal power at $z = 0$ (launch power). Note that backward Raman amplification and lumped amplification do not affect the NLI-limited SNR in the first half of the link, as both signal and noise powers are amplified by the same factor. The results are presented in Fig. 9(b). Significant NLI noise occurs within the first 30 km of transmission, over which distance the forward pumps enhance the signal power in the longer wavelength S-band and C-band, resulting in a lower $\mathrm{SNR}_{\mathrm{NLI,FW}}$ in these wavelengths, approximately 20 dB. The L-band experiences less NLI noise due to the lower launch power of 8.6 dBm in the L-band when applying the launch power tilt. The NLI noise induced by the power gain provided by the backward Raman pumps is negligible in this scenario, with an $\mathrm{SNR}_{\mathrm{NLI,BW}}$ exceeding 40 dB, due to the extremely low signal power after long-distance transmission. Thus, the NLI performance is primarily constrained by forward pumping.

Figure 9(c) summarises the contributions of the different noise sources to the total SNR, and compares the model prediction with the experimental results. Across most of the wavelength regions, ASE noise is the dominant noise source. However, NLI noise limits the total SNR in the longest wavelength S-band and the shortest wavelength C-band, where peak gain was provided by the Raman pumps. Excluding the negative SNRs in the shortest S-band channels, the averaged SNR error between model prediction and measured result across the remaining 479 channels is only 0.759 dB. The residual discrepancy is attributed to the accuracy of the power evolution calculation, which shows slight discrepancies between 1500 nm to 1540 nm in Fig. 8. The wavelength-dependence of the optical components, such as WDM couplers, isolators and amplifier noise figures, can also affect the model prediction result. Specifically in unrepeatered systems, the NLI noise from high power signals only occurs at the beginning of the fibre, where the impact of dispersion is not very strong. In such cases, the perturbative NLI approximation can sometimes model the system more effectively without Raman amplification. However, as shown in Fig. 9, the NLI noise induced by Raman amplification becomes comparable to the ASE noise level in parts of the S- and C-bands. In this scenario, the GN approach can accurately estimate both the NLI and Raman-induced ASE. Despite the dominance of ASE noise in some regions, the SNR modelling gives a breakdown of the different noise contributions in an unrepeatered link, explaining the reasons for SNR degradation along the fibre and highlighting the joint effect of Raman-induced ASE noise, lumped amplification-induced ASE noise, and bi-directional Raman pump-induced NLI noise. In conclusion, ASE noise

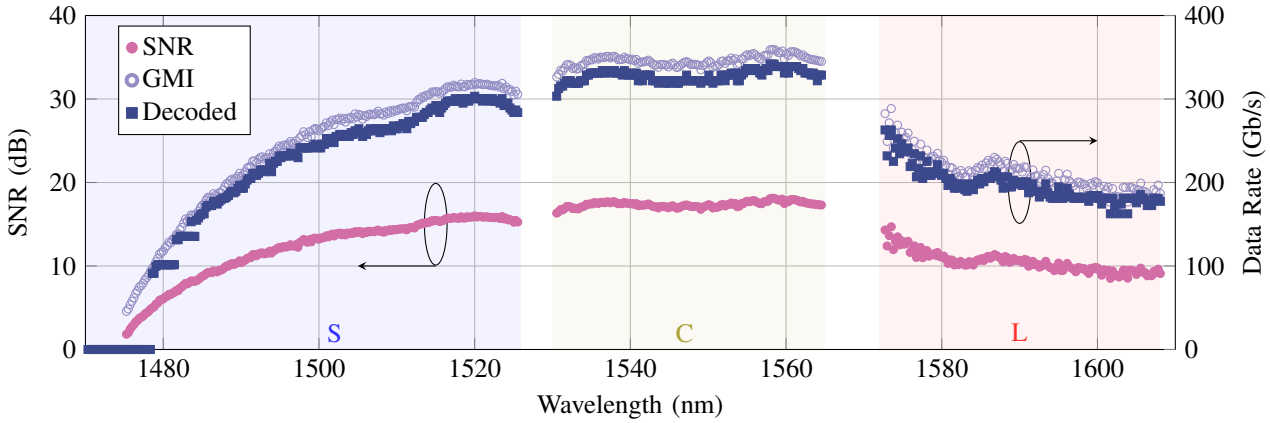

Fig. 10: Transmission SNR and data rate (estimated from GMI and after decoding) measurements for 228×S-, 132×C- and 130×L-band channels after 223 km unrepeatered transmission.

is the primary factor limiting transmission quality in unrepeatered systems, while NLI noise resulting from increased signal power due to forward Raman amplification can also degrade the SNR at wavelengths with peak Raman gain.

The achievable data rate was estimated using the Shannon capacity theorem, with the pilot overhead deducted, based on the SNRs for all transmission channels, calculated from the ISRS GN model. Without Raman amplification, the model predicts a throughput of only 23.58 Tb/s, entirely limited by the ASE from the significant lumped gain required to overcome approximately 40 dB of power loss. With Raman amplification, the estimated throughputs are 85.24 Tb/s with forward-only pumping and 64.80 Tb/s with backward-only pumping. Bi-directional Raman amplification is calculated to further increase the throughput to 130.98 Tb/s, representing 53.7 % and 102.1 % improvements compared to the forward-only and backward-only Raman configurations, respectively. This throughput is lower than the 155.3 Tb/s predicted during the optimisation process because the modelling further accounts for nonlinear interference and transceiver noise. Further improvement is also possible by using different types of fibres to balance the fibre attenuation and the Raman pump depletion. For example, using ULL fibre throughout the entire transmission link would reduce the backward Raman gain due to the presence of the water peak in the E-band, but the transmitted signal, on the other hand, would benefit from lower attenuation, which, according to the model, could result in similar or even higher throughput.

The received SNR was measured for each channel after pilot-based DSP. Data rates were then estimated from the GMI and after decoding, with the pilot overhead deducted. DVB-S2X LDPC codes were used with adaptive code rate and code-rate puncturing. The measured results are presented in Fig. 10. At the shortest S-band wavelengths, the OSNR is too low to transmit data at a significant rate, especially when the SNR is less than 5 dB and the GMI is nearly zero. The lowest decoding rate used in the experiment was 0.25, thus the channels with lower normalised GMI are unable to be recovered free of error. Deducting the unusable channels and the gap between optical bands, the total optical bandwidth used is approximately 121 nm. Data rates of 49.31 Tb/s, 45.66 Tb/s, and 27.65 Tb/s were estimated from GMI for the S-, C-, and L-bands respectively, totalling 122.62 Tb/s and 113.95 Tb/s before and after decoding, respectively. The GMI estimated the throughput using bit-metric decoding under practical conditions, and the gap to the model estimation of 130.98 Tb/s is due to slight mismatches in power evolution predictions and the inherent difference between real transmission systems and the ideal Shannon capacity. Further improvement of the system is possible by applying lower cardinality constellations, such as 16 QAM or QPSK, for the shorter wavelength S-band channels, which could potentially increase the data rate by approximately 1.2 Tb/s.

V. Conclusion

An ultra-wide band (121 nm, 15.6 THz) unrepeatered transmission link of 223 km with a total throughput of 122.62 Tb/s (113.95 Tb/s after decoding) was experimentally demonstrated using bidirectional Raman amplification and doped fibre amplifiers. The launched signal power profile and Raman pump powers were optimised using a differential evolution algorithm to mitigate the interchannel stimulated Raman scattering effect. The transmission system is modelled using a closed-form ISRS GN model to reproduce the signal power evolution along the link and predict the noise contributions to the SNR, showing that the unrepeatered system is dominated by the ASE noise arising from Raman and lumped amplification, with potential further reduction in the SNR due to nonlinear interference noise arising from forward Raman amplification increasing the signal power. The combination of hybrid amplification scheme, adaptive constellation shaping and decoding, and system optimisation achieved a record high data rate for unrepeatered standard single-mode fibre links over 200 km. These results highlight the potential of S+C+L band transmission to significantly enhance the capacity of unrepeatered transmission systems. Further increases in S-band transmission throughput could be achieved by using forward Raman pumps at shorter wavelengths, such as 1365 nm, and by employing signals with low modulation cardinality and/or stronger FEC at wavelengths suffering low SNR.

REFERENCES

[1] J. Chesnoy, *Undersea fiber communication systems*, 2nd ed. Amsterdam: Academic press, 2015.

[2] B. J. Puttnam, R. S. Luís, G. Rademacher, M. Mendez-Astudillio, Y. Awaji, and H. Furukawa, "S-, C- and L-band transmission over a 157 nm bandwidth using doped fiber and distributed Raman amplification," *Opt. Express*, vol. 30, no. 6, pp. 10 011–10 018, 2022.

[3] R. S. Luís, B. J. Puttnam, G. Rademacher, M. van den Hout, G. D. Sciullo, D. Orsuti, C. Okonkwo, C. Antonelli, J. Sakaguchi, and H. Furukawa, "Wideband unrepeatered transmission using doped Tellurite-fiber amplifiers," *J. Lightw. Technol.*, pp. 1–7, 2024.

[4] A. Ghazisaeidi, A. Arnould, M. Ionescu, V. Aref, H. Mardoyan, S. Etienne, M. Duval, C. Bastide, H. Bissessur, and J. Renaudier, "99.35 Tb/s ultra-wideband unrepeated transmission over 257 km using semiconductor optical amplifiers and distributed Raman amplification," *J. Lightw. Technol.*, vol. 40, no. 21, pp. 7014–7019, 2022.

[5] H. Bissessur, C. Bastide, S. Dubost, A. Calsat, F. Hedaraly, P. Plantady, and A. Ghazisaeidi, "Unrepeatered transmission of 29.2 Tb/s over 295 km with probabilistically shaped 64 QAM," in *Proc. Eur. Conf. Opt. Commun.*, Roma, Italy, 2018, paper Th1G.4.

[6] I. F. de Jauregui Ruiz, N. Abdukerim, J. van Weerdenburg, T. Gerard, F. J. V. Caballero, J. M. Buset, and L. Galdino, "66.8 Tb/s real-time C+L unrepeatered transmission over 301 km using forward and backward Raman amplification," in *Proc. Opt. Fiber Commun. Conf.* San Diego, California, USA: Optica Publishing Group, 2024, paper W3F.4.

[7] R. S. Luis, B. J. Puttnam, G. Rademacher, Y. Awaji, and H. Furukawa, "Demonstration of a 90 Tb/s, 234.8 km, C+L band unrepeatered SSMF link with bidirectional Raman amplification," *Opt. Express*, vol. 30, no. 8, pp. 13 114–13 120, 2022.

[8] D. Chang, W. Pelouch, P. Perrier, H. Fevrier, S. Ten, C. Towery, and S. Makovejs, "150 x 120 Gb/s unrepeatered transmission over 409.6 km of large effective area fiber with commercial Raman DWDM system," *Opt. Express*, vol. 22, no. 25, pp. 31 057–31 062, 2014.

[9] Y.-K. Huang, E. Ip, S. Zhang, F. Yaman, J. D. Downie, W. A. Wood, A. Zakharian, J. Hurley, S. Mishra, Y. Aono, E. Mateo, and Y. Inada, "20.7-Tb/s repeater-less transmission over 401.1-km using QSM fiber and XPM compensation via transmitter-side DBP," in *Proc. Opt-Electronics Commun. Conf*, Niigata, Japan, 2016, paper PD1-4.

[10] H. Zhang, B. Zhu, T. Pfau, M. Aydinlik, N. Nadarajah, S. Park, J. C. Geyer, L. Chen, R. Aroca, C. Doerr, and C. Rasmussen, "Real-time transmission of single-carrier 400 Gb/s and 600 Gb/s 64QAM over 200km-span link," in *Proc. Eur. Conf. Opt. Commun.*, Dublin, Ireland, 2019, paper Tu.2.D.

[11] J. Li, A. Zhang, L. Feng, Y. Liu, X. Huo, F. Yan, Y. Yang, H. Wang, L. Wang, L. Hu, T. Dai, Y. Liu, H. Chen, J. Chen, Y. Yu, L. Li, J. Wu, and L. Xiong, "Real-time unrepeatered extended C-band transmission of 16-Tb/s over 420-km (73.2-db) and 24-Tb/s over 390-km (67.7-dB) with field-deployed submarine cable," in *Asia Commun. Photonics Conf.*, Shenzhen, China, 2022, pp. 656–658.

[12] J. Wu, J. Yu, J. Liu, Q. Hu, M. Duan, W. Wang, C. Huang, H. Long, S. Sun, M. Tan, L. Huang, and J. Xu, "Real-time 33.6 Tb/s (42 × 800 Gb/s) unrepeatered transmission over 302 km using ROPA system," in *Proc. Opt. Fiber Commun. Conf.*, San Diego, California, USA, 2023, paper Tu2G.7.

[13] A. Busson, H. Bissessur, D. Kravchenko, F. Hedaraly, and J. Esparza, "Unrepeatered C-band transmission of 35.5 Tb/s capacity over 291 km using 128 GBd DP-16-QAM," in *Proc. Opt. Fiber Commun. Conf.* San Diego, California, USA: Optica Publishing Group, 2023, paper Tu2G.4.

[14] S. Almonacil, H. Bissessur, H. Mardoyan, A. Busson, A. Ghazisaeidi, D. Kravchenko, and J. Renaudier, "C-band unrepeated transmission system over 291-km at net throughput of 41.3-Tbps without ROPA," in *Proc. Eur. Conf. Opt. Commun.*, Glasgow, Scotland, UK, 2023, paper Th.B.2.3.

[15] J. Renaudier, A. Arnould, A. Ghazisaeidi, D. Le Gac, P. Brindel, E. Awwad, M. Makhsiyan, K. Mekhazni, F. Blache, A. Boutin *et al.*, "Recent advances in 100+ nm ultra-wideband fiber-optic transmission systems using semiconductor optical amplifiers," *J. Lightw. Technol.*, vol. 38, no. 5, pp. 1071–1079, 2020.

[16] F. Hamaoka, M. Nakamura, T. Sasai, S. Sugawara, T. Kobayashi, Y. Miyamoto, and E. Yamazaki, "110.7-Tb/s single-mode-fiber transmission over 1040 km with high-symbol-rate 144-GBaud PDM-PCS-QAM signals," in *Proc. Opt. Fiber Commun. Conf.* San Diego, California, USA: Optica Publishing Group, 2024, paper Tu3E.6.

[17] P. Poggiolini, "The GN model of non-linear propagation in uncompensated coherent optical systems," *J. Lightw. Technol.*, vol. 30, no. 24, pp. 3857–3879, 2012.

[18] D. Semrau, R. I. Killey, and P. Bayvel, "A closed-form approximation of the Gaussian noise model in the presence of inter-channel stimulated Raman scattering," *J. Lightw. Technol.*, vol. 37, no. 9, pp. 1924–1936, 2019.

[19] Y. Jiang and P. Poggiolini, "CFM6, a closed-form NLI EGN model supporting multiband transmission with arbitrary Raman amplification," *arXiv preprint arXiv:2405.08512*, 2024.

[20] H. Buglia, M. Jarmolovičius, L. Galdino, R. I. Killey, and P. Bayvel, "A closed-form expression for the Gaussian noise model in the presence of Raman amplification," *J. Lightw. Technol.*, vol. 42, no. 2, pp. 636–648, 2024.

[21] H. Buglia, E. Sillekens, L. Galdino, R. Killey, and P. Bayvel, "Throughput maximisation in ultra-wideband hybrid-amplified links," in *Proc. Opt. Fiber Commun. Conf.* San Diego, California, USA: Optica Publishing Group, 2024, paper Tu3H.5.

[22] J. Yang, R. Aparecido, H. Buglia, P. Hazarika, E. Sillekens, R. Sohanpal, M. Tan, D. Pratiwi, R. S. Luis, B. J. Puttnam, Y. Wakayama, W. Forysiak, P. Bayvel, and R. I. Killey, "122.6 Tb/s S+C+L band unrepeated transmission over 223 km link with optimised bidirectional Raman amplification," in *Proc. Opt. Fiber Commun. Conf.* San Diego, California, USA: Optica Publishing Group, 2024, paper W4D.5.

[23] B. Geiger, E. Sillekens, F. Ferreira, R. Killey, L. Galdino, and P. Bayvel, "On the performance limits of high-speed transmission using a single wideband coherent receiver," *J. Lightw. Technol.*, vol. 41, no. 12, pp. 3816–3824, 2023.

[24] E. Sillekens, G. Liga, D. Lavery, P. Bayvel, and R. I. Killey, "High-cardinality geometrical constellation shaping for the nonlinear fibre channel," *J. Lightw. Technol.*, vol. 40, no. 19, pp. 6374–6387, 2022.

[25] D. J. Elson, G. Saavedra, K. Shi, D. Semrau, L. Galdino, R. Killey, B. C. Thomsen, and P. Bayvel, "Investigation of bandwidth loading in optical fibre transmission using amplified spontaneous emission noise," *Opt. Express*, vol. 25, no. 16, pp. 19 529–19 537, 2017.

[26] J.-X. Cai, Y. Hu, A. Turukhin, M. V. Mazurczyk, M. Paskov, H. G. Batshon, C. R. Davidson, M. Bolshtyansky, and D. G. Foursa, "On the effects of transmitter induced channel correlation in broadband WDM transmission," in *Proc. Opt. Fiber Commun. Conf.*, San Diego, California, USA, 2018, paper Th1C.1.

[27] J. Cho, X. Chen, S. Chandrasekhar, G. Raybon, R. Dar, L. Schmalen, E. Burrows, A. Adamiecki, S. Corteselli, Y. Pan, D. Correa, B. McKay, S. Zsigmond, P. Winzer, and S. Grubb, "Trans-atlantic field trial using probabilistically shaped 64-QAM at high spectral efficiencies and single-carrier real-time 250-Gb/s 16-QAM," in *Proc. Opt. Fiber Commun. Conf.* Los Angeles, California, United States: Optica Publishing Group, 2017, paper Th5B.3.

[28] L. Galdino, A. Edwards, W. Yi, E. Sillekens, Y. Wakayama, T. Gerard, W. S. Pelouch, S. Barnes, T. Tsuritani, R. I. Killey, D. Lavery, and P. Bayvel, "Optical fibre capacity optimisation via continuous bandwidth amplification and geometric shaping," *IEEE Photon. Technol. Lett.*, vol. 32, no. 17, pp. 1021–1024, 2020.

[29] Y. Wakayama, T. Gerard, E. Sillekens, L. Galdino, D. Lavery, R. I. Killey, and P. Bayvel, "2048-QAM transmission at 15 GBd over 100 km using geometric constellation shaping," *Opt. Express*, vol. 29, no. 12, pp. 18 743–18 759, 2021.

[30] A. Alvarado, T. Fehenberger, B. Chen, and F. M. J. Willems, "Achievable information rates for fiber optics: Applications and computations," *J. Lightw. Technol.*, vol. 36, no. 2, pp. 424–439, 2018.

[31] Digital Video Broadcasting (DVB), "Second generation framing structure, channel coding and modulation systems for broadcasting, interactive services, news gathering and other broadband satellite applications; Part 2: DVB-S2 extensions (DVB-S2X)," in *ETSI Standard SIST EN 302 307-2 V1.2.1:2020, European Telecommunications Standards Institute (ETSI), Sophia-Antipolis, France*, 2021.

[32] K. V. Price, "Differential evolution," in *Handbook of optimization: From classical to modern approach*, I. Zelinka, V. Snasel, and A. Abraham, Eds. Springer, 2013, pp. 187–214.

[33] M. F. Ahmad, N. A. M. Isa, W. H. Lim, and K. M. Ang, "Differential evolution: A recent review based on state-of-the-art works," *Alex. Eng. J.*, vol. 61, no. 5, pp. 3831–3872, 2022.

[34] V. V. Ivanov, P. M. Sterlingov, S. K. Mishra, J. D. Downie, and S. Makovejs, "Effective area tilt impact in S+C+L band long-haul fiber optic transmission systems," in *Proc. Opt. Fiber Commun. Conf.* San Diego, California, USA: Optica Publishing Group, 2022, paper W3E.4.